Light and hydrologic variability as drivers of stream biofilm dynamics in a flume experiment

Serena Ceola,[1] Enrico Bertuzzo,[1] Lorenzo Mari,[1,2] Gianluca Botter,[3] Iris Hödl,[4] Tom J. Battin,[4,5] Marino Gatto[2] and Andrea Rinaldo[1,3]*

[1] *Laboratory of Ecohydrology ECHO/IIE/ENAC, École Polytechnique Fédérale Lausanne, Lausanne, Switzerland*
[2] *Dipartimento di Elettronica e Informazione, Politecnico di Milano, Milano, Italy*
[3] *Dipartimento di Ingegneria Civile, Edile, ed Ambientale, Università degli Studi di Padova, Padova, Italy*
[4] *Department of Limnology, University of Vienna, Vienna, Austria*
[5] *WasserCluster Lunz, Interuniversity Center for Aquatic Ecosystem Research, Lunz am See, Austria*

ABSTRACT

We run a comparative study of the results of flume experiments and several dynamic models reproducing the effects of streamflow variability on biofilm (i.e. periphyton) temporal dynamics. During the experiment, two contrasting flow regimes, characterised by a constant and a time-varying discharge temporal sequence, and four different light conditions (from 90% to 27% transmission of incident light) were performed to test the effects of availability and temporal variability of light and streamflows on biofilm growth. Several model formulations, describing growth and loss dynamics, have been explored in order to assess the relevant processes that controlled biofilm temporal pattern. Model identification criteria were used to identify the most suitable model, in which the growth rate is found to be dependent on density-limitation dynamics coupled with a saturating light effect, while the loss rate is linearly proportional to the discharge conditions experienced in the flumes. This model formulation proved able to reproduce remarkably well the observed biofilm dynamics. In order to analyse the stationary behaviour of the best-performing model reproducing biofilm biomass dynamics, we also run a long-term simulation, where no significant biomass differences between the constant and stochastic flow regimes were detected.

KEY WORDS stream biofilm; dynamic model; hydrology; stream ecology; light; streamflow

Received 27 July 2012; Revised 11 October 2012; Accepted 15 November 2012

INTRODUCTION

Stream biofilms are a key component of stream ecosystems, where they significantly contribute to benthic primary production and ecosystem respiration (Battin *et al.*, 2008). Biofilms are aggregations of microorganisms, algae and protozoa embedded in an extracellular polysaccharide matrix, attached to surfaces. Biofilms are at the base of the stream food chain (Saravia *et al.*, 1998), being the principal food resource for macroinvertebrates (McIntire, 1973; Allan and Castillo, 2007).

Biofilm development and temporal dynamics are mainly controlled by two different classes of abiotic factors: resources, such as light intensity, nutrient concentration and water temperature that regulate biomass growth, and disturbances related to hydraulic conditions that contribute to biomass loss (Stevenson, 1983; Biggs, 1996; Biggs *et al.*, 1998; Tuji, 2000; Hondzo and Wang, 2002; Allan and Castillo, 2007). Therefore, biofilm biomass depends at any time on the balance between these controlling variables. Although nutrient concentration and water temperature are commonly considered relevant factors controlling the metabolic activity of benthic organisms (Allan and Castillo, 2007), light availability and hydrodynamics, among all abiotic variables, exert a key role on stream biofilm dynamics (Biggs and Close, 1989; DeNicola and McIntire, 1991).

More specifically, light intensity, which typically changes along the fluvial continuum (Vannote *et al.*, 1980) as a function of vegetation coverage and water turbidity (Julian *et al.*, 2008), is known to control primary production (Hill *et al.*, 1995). Light-limitation effects can be found at low light intensity, because a minimum light availability is needed for biomass accrual because of photosynthesis, even though phototrophic biofilms may acclimate to dark conditions, showing an increasing photosynthetic efficiency at low light levels (Stevenson *et al.*, 1996). On the other hand, extremely high light conditions may also limit biomass growth because of photo-inhibition (Hill *et al.*, 1995).

Discharge influences biofilm biomass, by either enhancing nutrient availability with increasing flow velocity or mechanically inducing biomass detachment (Biggs, 1996; Stevenson *et al.*, 1996; Biggs *et al.*, 2005). Discharge, flow velocity, average bottom shear stress and shear velocity have

*Correspondence to: Andrea Rinaldo, Laboratory of Ecohydrology ECHO/IIE/ENAC, École Polytechnique Fédérale Lausanne, Lausanne, Switzerland. E-mail: andrea.rinaldo@epfl.ch

been interchangeably considered the controlling hydraulic variables of periphyton biomass development (Biggs *et al*., 1990; Horner *et al*., 1990; Jowett and Duncan, 1990; Power *et al*., 1995a, 1995b; Biggs, 1996; Saravia *et al*., 1998; Hondzo and Wang, 2002). For example, Horner *et al*. (1990) argued that important biomass losses usually take place in the presence of flow velocities greater than the mean velocity under which the biofilm grew. Similarly, Hondzo and Wang (2002) proposed a threshold shear velocity value of about $0.7\,\mathrm{cm\,s^{-1}}$ for periphyton biomass to suffer from significant shear-induced losses. In these circumstances, cascade bottom-up effects may affect higher trophic levels of the river food chain, whose length mainly depends on discharge temporal variability (Marks *et al*., 2000; Sabo *et al*., 2010). Indeed, streamflow is considered the master variable that drives fluvial ecological processes (Power *et al*., 1995b; Poff *et al*., 1997; Richter *et al*., 1996; Richter *et al*., 1997). Streamflow is the outcome of form and function of the river basin, blending rainfall, climate, land use and geomorphological processes (e.g. Rinaldo and Rodriguez-Iturbe, 1996; Rinaldo *et al*., 2006), whose intrinsic stochasticity is driven by natural heterogeneity and the time-variable rainfall patterns. Climate change and human activity may influence and alter discharge magnitude and frequency, with consequent effects on fluvial ecosystem spatial extension and food chain length (Jackson *et al*., 2001; Allan and Castillo, 2007; Poff *et al*., 2007; Botter *et al*., 2010; Sabo *et al*., 2010; Kupferberg *et al*., 2012).

Several simulation models, taking into account the effects of the aforementioned environmental factors (or a combination of them), have been developed in order to reproduce periphyton biomass dynamics in experimental flumes or natural streams. Momo (1995), for instance, provided a logistic growth approach to describe biofilm evolution, which accounted also for flow-induced detachment, while Saravia *et al*. (1998) presented a model on the basis of light intensity, nutrients and flow velocity. McIntire's (1973) model analysed growth dynamics in terms of light availability, water temperature and nutrient concentration, whereas loss dynamics were governed by scouring, flow velocity, water temperature and grazing activity. However, the analysis and the modelling of the effects of a time-varying discharge sequence on biofilm growth in a controlled experiment are still lacking.

Here, we analyse the effects of light availability and flow regime on biofilm biomass dynamics obtained from a 2-month flume experiment, in which two contrasting flow regimes and four different light conditions were explored. Specifically, all measured data refer to ungrazed conditions (i.e. absence of macroinvertebrate grazing activity). Respectively, eight and five different models describing growth and detachment dynamics (i.e. 40 model combinations in total) have been tested against measured data.

The paper is organised as follows. The experimental campaign, the different models for biofilm growth and loss due to detachment, the parameter calibration and model selection procedures are described in the Material and Methods section. Modelling results are presented in the Results section, while a discussion and final remarks are reported in the Discussion and Conclusions section.

MATERIAL AND METHODS

Experiment description

Experimental equipment. The experiments were conducted at the WasserCluster Lunz, Lunz am See (Austria), from mid-July to mid-September 2011. In total, 24 outdoor flumes, each 3 m long, 0.1 m deep and 0.05 m wide, with a slope of 0.3%, operated in a once-through flow mode, were used to perform biofilm growth under two alternative discharge treatments and four different light regimes, with three replicates for each treatment combination (Figure 1). Half (i.e. 12) of the flumes experienced a time-varying

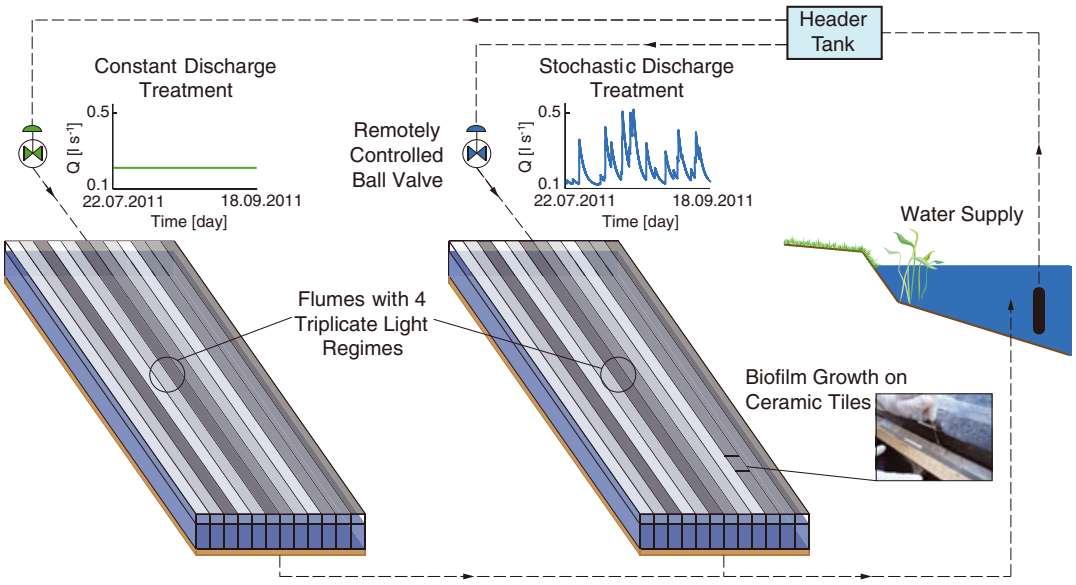

Figure 1. Schematic representation of the experimental setup, with details on performed discharge and light treatments, and biofilm growth on ceramic tiles.

discharge sequence, $Q(t)$, derived from a stochastic process that reproduces relevant streamflow dynamics in a river basin (Botter *et al.*, 2007c, Section 2). The remaining 12 flumes, characterised by a constant flow regime equal to the average discharge of the stochastic process, were used as controls. Light availability [L, expressed as photosynthetically active radiation (PAR)], as a major control on biofilm growth, was manipulated using four distinct lighting filters, which provided different light intensities without changing light colour. In particular, colour correction Neutral Density foils 226, 298, 209 and 210 were placed on the top of the flumes in order to perform light levels equal to 90%, 65%, 50% and 27% transmission of incident PAR, respectively. Flumes were thus characterised by average (±standard deviation) daily maximal intensities of PAR of 1130 ± 220, 864 ± 195, 625 ± 141 and $359 \pm 81\ \mu E\,m^{-2}\,s^{-1}$ in the respective light treatments, lying within the range of maximal daily PAR values (from 131 to $1753\ \mu E\,m^{-2}\,s^{-1}$, $1142 \pm 384\ \mu E\,m^{-2}\,s^{-1}$). The random placement of lighting foils was identical for both discharge treatments. Low-porosity unglazed ceramic tiles, 47.6 ± 0.2 mm long and wide, were placed at the bottom of each flume as a substratum for biofilm growth (Lamberti and Resh, 1985).

Raw and unfiltered water was supplied through a submerged pump, with temperature ranging from 10.5 to 13.9 °C. A header tank (4.3 m^3) received the pumped water that flowed into two pipes, one for each discharge treatment (external diameter 90 mm – Diameter Nominal 80 mm, d90-DN80) placed at the bottom of the tank, and then entered two intermediate tanks (each 0.35 m^3) that supplied the 12 + 12 flumes. The water levels of the intermediate tank and corresponding flumes were equal in order to guarantee identical hydraulic conditions for all flumes belonging to the same discharge treatment. To enhance uniform flow conditions and sustain water level, three nets were located in correspondence to the flume inlet, 1.75 m downstream, and in correspondence to the flume outlet. The flume outlet was open, and water freely flowed into a small channel. All the components of the experimental setup were covered to prevent incoming rainfall, leaves and insects.

Streamflow probability distribution function and experimental discharge treatments. The discharge sequence used during the experiment is a Monte Carlo realisation of a stochastic process, which has been chosen to mimic the relevant streamflow dynamics in river basins. In particular, the streamflow dynamics are assumed to be driven by Poissonian random jumps representing the streamflow increment produced by rainfall events capable of mobilising the underlying drainage catchment and by exponential decays representing the recessions in between the events (Botter *et al.*, 2007c). The above stochastic scheme is based on the following assumptions:

1. Daily rainfall events are modelled as a Poisson process with frequency λ_P (T^{-1});
2. daily rainfall depths are exponentially distributed with mean α (L);
3. daily soil moisture dynamics in the near-surface soil layer are governed by infiltration, soil moisture dependent evapotranspiration and instantaneous deep percolation events effectively contributing to streamflow production;
4. the sequence of events contributing to streamflow production are modelled as a Poisson process with frequency $\lambda < \lambda_P$ (T^{-1});
5. the volumes released from the near-surface soil layer are then released from the soil to the channel network according to an exponential response function with mean response time $1/k$ (T).

The probability distribution of streamflows, Q ($L^3\,T^{-1}$), resulting from the above model can be analytically expressed as (see Botter *et al.*, 2007b, 2007c, for further details):

$$P(Q) = \frac{(\alpha k A)^{-1}}{\Gamma\left(\frac{\lambda}{k}\right)} \left(\frac{Q}{\alpha k A}\right)^{\frac{\lambda}{k}-1} e^{-\frac{Q}{\alpha k A}} \qquad (1)$$

where A (L^2) represents the catchment area and $\Gamma(x)$ is the complete gamma function of argument x. The streamflow pdf given by Equation (1) has been proved able to reproduce remarkably well the observed behaviour of many catchments throughout the world, characterised by different climatic and morphologic attributes (Botter *et al.*, 2007a, 2008; Ceola *et al.*, 2010). For our experimental campaign, conducted in a pre-alpine area (Oberer Seebach), we selected the parameter values aiming at the reproduction of typical features of pre-alpine streams. Therefore, we have chosen the values $\lambda = 0.6\ day^{-1}$ and $k = 0.5\ day^{-1}$. In addition, given that streamflow magnitude depends on the product αA (L^3), we chose a plausible value of this quantity in order to generate a discharge temporal sequence that fitted the flume dimensions (i.e. that produced viable shear velocities and a reasonable range of water depths that allowed proper measure and avoided scale effects). A constant discharge treatment, with magnitude equal to the average of the stochastic flows, was used as a control. To measure and implement the temporal discharge sequences, a propeller flow metre and a ball valve were placed in each pipe. In particular, a computer-controlled electric ball valve was used to realise a controlled stochastic discharge sequence, while a manual ball valve was used to regulate the constant discharge. To this aim, a suitable computer-controlled system was developed using National Instruments LabVIEW™ software.

Biofilm growth experiment. Biofilm biomass was measured as total organic matter, expressed as ash-free dry mass ($mg\,cm^{-2}$). One sampling tile per flume was taken in intervals of 2 to 7 days and then replaced by a new white tile. Biofilms on each sampled tile were completely removed using sterile razor blades. The suspensions of scraped biofilm and MilliQ water were vortexed and sonicated and subsequently filtered onto pre-ashed (450 °C, 5 h) glass-fibre filters (Whatman) to determine biofilm organic matter.

Additional experimental measurements. Measurements of flume water level and temperature and header tank water temperature were taken on a daily basis. Flow profiles in the test areas were carefully measured, and uniform flow conditions (i.e. constant water depth) were insured. Measurements of cross-sectional average bottom shear stress exerted on the wetted perimeter were derived from flume discharge and water level. In the uniform flow conditions maintained here, the shear stress, τ, can be expressed as follows:

$$\tau = \gamma_w R_h s \tag{2}$$

where γ_w ($MT^{-2}L^{-2}$) is the specific weight of water; R_h (L) is the hydraulic radius, defined as the ratio of wetted area and perimeter (in the case at hand of rectangular cross section, $R_h = By/(B+2y)$, where B (L) and y (L) are the flume width and depth, respectively); and s is the constant flume slope. The resulting relation between flume discharge, Q, and bottom shear stress, τ, reads as

$$\tau = aQ^{\delta} \tag{3}$$

where the exponent $\delta = 0.33$ is derived from the experimental rating curve. Table I reports the performed hydraulic conditions in the flumes for both discharge treatments expressed in terms of discharge Q, water depth y, flow velocity v, shear stress τ, shear velocity u_* (i.e. $u_* = \sqrt{\tau/\rho}$, where ρ is the fluid density) and Reynolds number R_e.

The model

Biofilm biomass temporal dynamics was tested against a set of simulation models, aiming at the identification of possible controlling factors. Models were expressed by the basic form

$$\frac{dB}{dt} = rB - lB \tag{4}$$

where B is the biofilm biomass; r represents the net biofilm growth rate, embedding also intrinsic biomass decay and discharge-independent detachment; and l represents the hydraulic-induced loss rate.

For our modelling analysis, we hypothesised that biofilm dynamics may be mainly influenced by the following three controlling factors:

1. light availability, influencing photosynthetic activity of biofilm algae;
2. space limitation in the flumes for biofilm growth, possibly driving density-dependent growth processes;
3. hydraulic conditions, controlling biomass loss.

Water temperature and nutrient concentration influences on biofilm dynamics have not been taken into account in the model formulation because of negligible temporal variation of these two abiotic controlling factors during the experiment.

Following the literature on biofilm growth dynamics (e.g. McIntire, 1973; Momo, 1995; Uehlinger *et al*., 1996; Saravia *et al*., 1998), biofilm growth can be expressed as follows (Table II): (i) a Malthusian model, characterised by an exponential increase of biomass through time (model R1); (ii) a light-dependent growth process (models R2–R4); (iii) a density-dependent growth process (model R5); and (iv) a density-dependent and light-dependent growth process, where equations R2–R4 have been coupled with R5 (models R6–R8). In particular, the influence of light availability on biofilm growth has been expressed following three alternative

Table I. Flume hydraulic conditions, expressed in terms of discharge, water depth, flow velocity, bottom shear stress, shear velocity and Reynolds number, for both discharge treatments.

	Stochastic flow treatment	Constant flow treatment
Discharge, Q ($l\,s^{-1}$)	0.12–0.51	0.21
Water depth, y (cm)	1.32–3.13	1.82
Flow velocity, v ($cm\,s^{-1}$)	18.59–32.70	22.96
Bottom shear stress, τ ($N\,m^{-2}$)	0.26–0.42	0.32
Shear velocity, u_* ($cm\,s^{-1}$)	1.59–2.02	1.76
Reynolds number, R_e	9788–40 888	18 408

Table II. Definition of the eight models describing the growth rate, r, used to reproduce measured biofilm biomass values.

Model name	Equation	Description
R1	r_0	Malthusian
R2	$r_0 L$	Light-dependent: linear relation
R3	$\frac{r_0 L}{k_L + L}$	Light-dependent: Monod-type equation
R4	$r_0 L e^{-k_L L}$	Light-dependent: Steele's equation
R5	$r_0(1 - r_1 B)$	Logistic (density-dependent)
R6	$r_0 L(1 - r_1 B)$	R2 with logistic density dependence
R7	$\frac{r_0 L}{k_L + L}(1 - r_1 B)$	R3 with logistic density dependence
R8	$r_0 L e^{-k_L L}(1 - r_1 B)$	R4 with logistic density dependence

formulations, also extensively applied in the analysis of phytoplankton (Ensign *et al.*, 2012) and sea-grass (Carr *et al.*, 2012) dynamics: a linear relation (model R2), a Monod-type equation (model R3), where k_L is the half saturation coefficient corresponding to the light availability at which r is one-half of its maximum, and Steele's equation (model R4), able to model the effect of possible photo-inhibition of biofilm growth at high incoming light radiation (Steele, 1962; Steele and Baird, 1962).

Biofilm detachment rate, as a function of hydraulic factors, was simulated by means of four alternative equations (Table III), some of which already employed by Saravia *et al.* (1998) and Fovet *et al.* (2010). More specifically, we assumed that the detachment rate may be proportional to discharge, following either a linear (model L2) or a power-law relation (model L3), or to shear stress, following either a linear (model L4) or a threshold-dependent power-law relation (model L5). In the latter case, with a formulation similar to sediment erosion models, biomass removal occurs only when a critical shear stress, equal to the biofilm resistance capacity, is reached. Note that the absence of hydraulic-induced biomass detachment is taken into account in model L1. We also considered a constant, discharge-independent loss relation, but in this case, the model parameters were strongly correlated. We thus decided to discard this class of models from our analysis. Overall, we simulated 40 different model combinations.

Parameter calibration and model selection

For each model, we estimated a unique set of parameters in order to reproduce as close as possible the time series of biofilm biomass obtained under all light and discharge treatments. Parameters were calibrated using an optimization approach based on Markov chain Monte Carlo (MCMC) methods. The MCMC algorithm allows for the sampling of the posterior probability distribution function of a desired probability distribution, which, in our case, is the joint probability distribution of the set of calibrating parameters (Gilks *et al.*, 1995). In particular, the differential evolution adaptive Metropolis (DREAM) algorithm (ter Braak and Vrugt, 2008) was adopted in order to simultaneously run multiple chains in parallel to completely explore the parameter space and flexibly adjust the scale and orientation of the jumping distribution using differential evolution (Storn and Price, 1997) and a Metropolis–Hastings update step (Metropolis *et al.*, 1953; Hastings, 1970). More specifically, we applied the DREAM_{ZS} variant of the DREAM algorithm, which in addition uses (i) sampling from past states examined by the Markov chains and (ii) a snooker update step (in addition to parallel update steps) to maximise the diversity of candidate points (Vrugt *et al.*, 2009). Uninformative flat prior distributions of parameter values were initialized before running $\mathcal{O}(10^5)$ iterations until convergence.

The goodness of each single simulation was evaluated as the residual sum of squares (RSS) between the measured and modelled biofilm biomass for all light and discharge treatments as follows:

$$\text{RSS} = \sum_{i=1}^{n} \left[B_i - \hat{B}_i\right]^2 \tag{5}$$

where B_i and $\hat{B}_i$ are the measured and simulated biofilm biomass values, respectively, and $n = 312$ is the total number of data points (13 sampling days $\times$ 4 light regimes $\times$ 2 discharge treatments $\times$ 3 independent replicates).

To compare the performances of the 40 candidate models describing the observed biofilm biomass dynamics, we used Akaike's information criterion (AIC) (Akaike, 1974). AIC is a model-selection approach that balances the goodness of fit and the complexity of the model, expressed as the number Θ of free parameters [i.e. number of parameters for each model, plus one residual variance parameter (Burnham and Anderson, 2002; Corani and Gatto, 2007)]. For each best-fit model, we quantified

$$\text{AIC} = 2\Theta + n\ln\left(\frac{\text{RSS}}{n}\right) \tag{6}$$

Because AIC values cannot be individually interpreted, being a function of Θ, they need to be rescaled with respect to the lowest AIC values (i.e. $\text{AIC}_{\min}$, which identifies the best model). Therefore, for each model, we calculated

$$\Delta_{\text{AIC}_i} = \text{AIC}_i - \text{AIC}_{\min} \tag{7}$$

where AIC_i is the AIC score correspondent to model i. Increasing Δ_{AIC} values identify less plausible models. A critical Δ_{AIC} threshold, above which models have no more applicable evidence, is usually fixed around 10 (Burnham and Anderson, 2002).

Table III. Definition of the five models describing the loss rate, l, used to reproduce measured biofilm biomass values.

Model name	Equation	Description
L1	—	No external loss
L2	$l_1 Q$	Discharge-dependent: linear relation
L3	$l_1 Q^{\eta}$	Discharge-dependent: power law
L4	$l_1 \tau$	Shear stress-dependent: linear relation
L5	$l_1(\tau - \tau_c)^{\eta}$	Shear stress-dependent: power law with threshold

RESULTS

The ability of the 40 candidate models to reproduce the observed data was analysed through the AIC test (see Table IV for number of calibrated parameters, root mean square error $\text{RMS} = \sqrt{\text{RSS}/n}$ values, AIC and Δ_{AIC} scores for each model). In particular, an interesting trend has been noted: Growth equations played a major role in describing biofilm dynamics compared with loss functions. The calibrated models could be thus easily pooled as a function of the growth equation, as shown in Table II. According to AIC test results, light-dependent and density-dependent growth functions are the best performing models for biofilm

Table IV. Summary of calibration results for the 40 tested models.

Growth model	Loss model	No. of parameters	RMS	AIC	Δ_{AIC}
R7	L2	4	0.0104	−914.75	—
R7	L1	3	0.0105	−914.09	0.66
R7	L3	5	0.0104	−913.52	1.23
R7	L4	4	0.0105	−911.84	2.91
R7	L5	6	0.0105	−908.09	6.66
R8	L1	3	0.0110	−888.24	26.51
R8	L3	5	0.0110	−886.78	27.97
R8	L2	4	0.0110	−885.98	28.77
R8	L4	4	0.0110	−885.60	29.15
R8	L5	6	0.0110	−882.24	32.51
R5	L1	2	0.0116	−861.20	53.55
R5	L2	3	0.0116	−861.14	53.60
R5	L3	4	0.0116	−859.69	55.06
R5	L4	3	0.0117	−859.03	55.72
R5	L5	5	0.0116	−855.22	59.53
R3	L5	5	0.0129	−802.62	112.13
R3	L4	3	0.0135	−784.37	130.38
R3	L3	4	0.0137	−772.22	142.53
R3	L2	3	0.0138	−769.97	144.78
R3	L1	2	0.0143	−753.96	160.79
R1	L5	4	0.0144	−748.07	166.68
R1	L4	2	0.0145	−747.40	167.34
R1	L2	2	0.0151	−728.23	186.52
R1	L3	3	0.0150	−728.02	186.73
R1	L1	1	0.0152	−725.99	188.76
R4	L5	5	0.0151	−719.61	195.14
R4	L3	4	0.0153	−715.05	199.70
R4	L1	2	0.0158	−704.62	210.13
R4	L2	3	0.0158	−702.43	212.32
R4	L4	3	0.0158	−702.29	212.46
R6	L1	2	0.0194	−597.06	317.69
R6	L2	3	0.0194	−594.49	320.26
R6	L4	3	0.0194	−593.91	320.84
R6	L3	4	0.0194	−593.06	321.69
R6	L5	5	0.0194	−591.06	323.69
R2	L5	4	0.0290	−383.95	530.80
R2	L1	1	0.0296	−379.98	534.77
R2	L3	3	0.0294	−379.03	535.72
R2	L2	2	0.0296	−377.60	537.15
R2	L4	2	0.0296	−377.31	537.44

growth. Light availability seems likely to be a limiting factor during the initial growth phase, while density-dependent effects, governed by space limitation in the flumes, may become important afterwards. On the basis of Δ_{AIC} scores, density-limited dynamics coupled with a Monod-type equation (R7), describing light influences on biomass growth, simulated remarkably well the data. Indeed, $\Delta_{AIC} < 10$ (i.e. critical threshold for model support) for all candidate models in this group. The alternative light-dependent and density-dependent group of models (R8) based on Steele's equation was characterised by slightly higher RMS values than those of R7 and consequently presented greater Δ_{AIC} values. Dynamic models based uniquely on density-dependent growth effects (R5) worked quite well in terms of RMS, while $\Delta_{AIC} >$ 50. The Malthusian (R1) and light-limited models, following either a Monod-type (R3) or Steele's (R4) equation, showed increasingly lower performances in terms of Δ_{AIC} scores. Both light-dependent and light-dependent and density-dependent growth functions based on a linear relation for light (R2 and R6, respectively) showed particularly high values of RMS and Δ_{AIC}. In either case, the model was not able to reproduce the observed biomass for all light and discharge treatments: A good fit was observed for the darkest condition, whereas for the other performed light regimes, the model sensibly overestimated the data. Concerning the description of biomass loss dynamics, within the same group of growth rate models, all the adopted loss functions showed a comparable behaviour, thus highlighting no clear distinctions among them. Quite interestingly, the threshold-dependent shear stress equation (L5) was the lowest performing loss function for all density-dependent growth models, while this equation showed the best results for all the remaining growth models.

Model parameters for the first-ranked model combination (R7–L2), and their probability distribution function, median and 5–95 percentiles, obtained from the last $\mathcal{O}(10^4)$ iterations of the Markov chain, are shown in Figure 2. In order to perform a sensitivity analysis of the model outcomes with

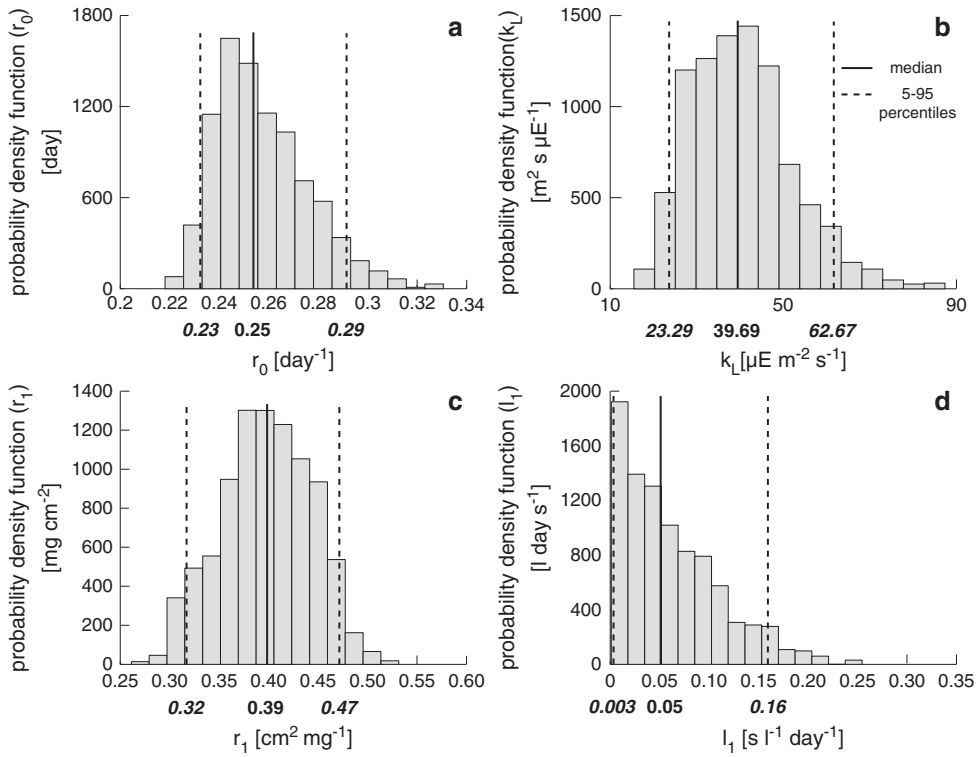

Figure 2. Probability distribution function of the parameters of the first-ranked model combination (R7–L2). Bold and italic bold numbers identify the median and the 5–95 percentiles derived from the parameter distribution, respectively.

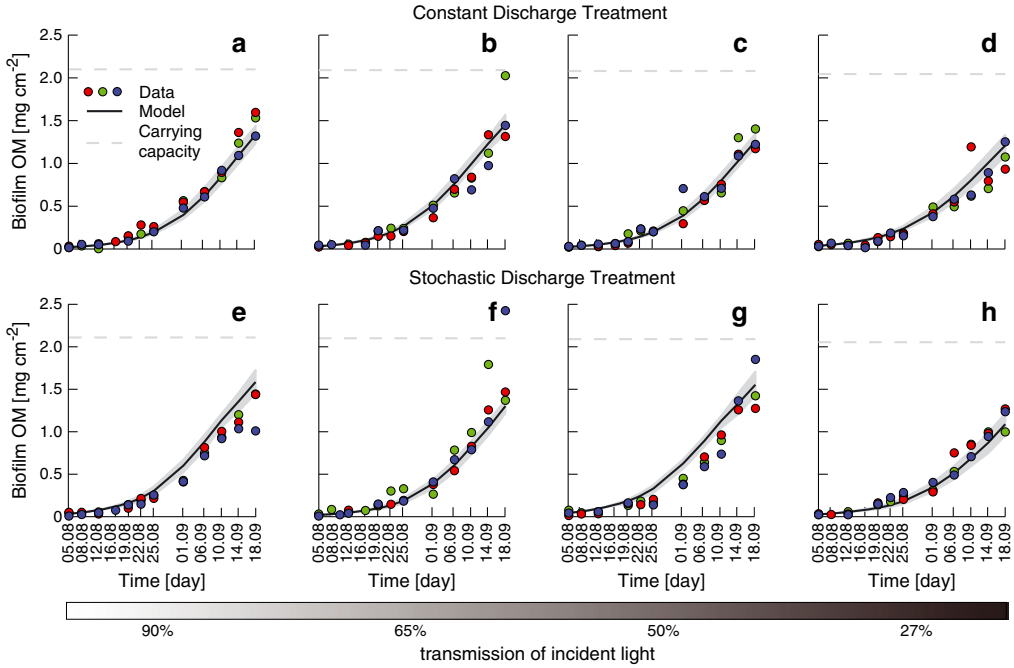

Figure 3. Simulation results from the first-ranked model combination R7–L2 against measured data, for each light and discharge treatment. The black solid line shows the behaviour of the best-set of model parameters, while the grey area quantifies the uncertainty related to parameter estimation (here represented by the minimum and maximum range of model simulations). The grey dashed line represents the biofilm carrying capacity, determined from Equation (8), where $\boldsymbol{Q} = <\boldsymbol{Q}(t)>$. Plots from a to d refer to the constant discharge treatment from 90% to 27% transmission of incident light. Analogously, plots from e to h refer to the stochastic discharge treatment. See also Supplementary Figure S1 in which the simulation results and the measured data are reported on a semi-log plot, thus revealing a non-exponential growth trend.

respect to variations of parameter values, from each set of explored parameters, sampled from the posterior probability distributions, the corresponding model simulations were evaluated. The minimum and maximum ranges of model simulations were consequently derived. Figure 3 reports measured biofilm biomass values (three replicate flumes with the same light and discharge treatments for each sampling day) and model outputs for the performed discharge and light

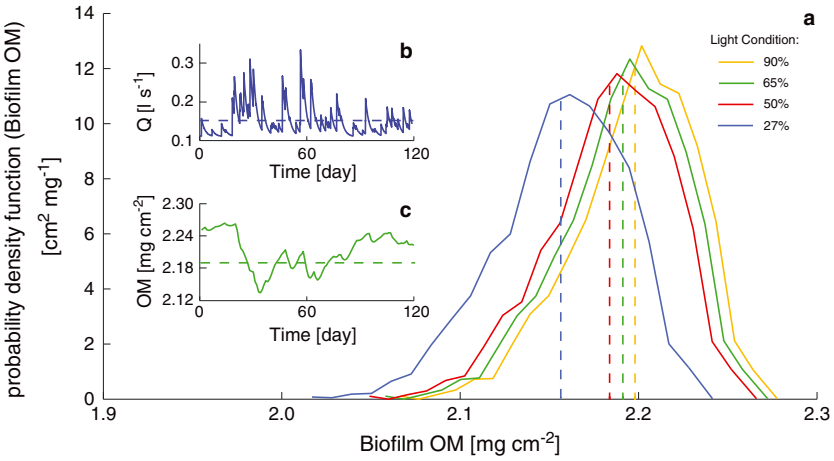

Figure 4. Biofilm biomass stationary behaviour from a long-term simulation. (a) Probability distribution function of biofilm biomass at stationarity ($t \to \infty$) for each light regime; (b) portion of the simulated discharge temporal sequence and (c) corresponding biofilm temporal dynamics at 65% of incoming light radiation. In each plot, solid lines and dashed lines represent the results from the stochastic and the constant discharge treatments, respectively.

treatments. The black solid line shows the performance of the best set of model parameters, while the grey area quantifies the uncertainty related to parameter estimation (here represented by the minimum and maximum range of model simulations).

Biomass values from the flume experimental campaign began to exhibit a saturating trend only towards the end of the experiment, moving slowly towards carrying capacity. The analytical expression for biomass carrying capacity can be derived according to our model formulation as follows. By substituting the expressions for growth and loss models (i.e. R7 and L2 relations, respectively) into Equation (4), the nontrivial equilibrium point (i.e. $dB/dt = rB - lB = 0$, for $t \to \infty$), which identifies the biofilm carrying capacity, is obtained as

$$B(t \to \infty) = \frac{1}{r_1} - \frac{l_1 Q}{r_0 r_1 L/(k_L + L)}, \qquad (8)$$

expressed as a function of light and discharge conditions. The carrying capacity values, evaluated for each light treatment from Equation (8), assuming $Q = < Q(t) >$, are reported in Figure 3.

In order to analyse the stationary behaviour of the biofilm dynamic model, an extended discharge temporal sequence with the same streamflow probability distribution, $p(Q)$, as the one used for the experimental stochastic discharge treatment, was generated and used as input for the biofilm dynamic model. Note that the parameters of $p(Q)$ were assumed to be constant over time, thus neglecting possible seasonal patterns in streamflow sequences. Analogously to the flume experiment, the average value of the stochastic discharge sequence was used to generate a long-term constant discharge regime. From the long-run simulation, for both discharge treatments and for light conditions ranging between 90% and 50% transmission of incident PAR, nearly 120 days were necessary to approach the stationary state (i.e. carrying capacity). The darkest light regime (27% transmission) required almost 30 days more (i.e. 150 days). Discharge temporal variability, embedded in the dynamic model through a linear relation, led to biofilm biomass fluctuations around the biomass value observed under the constant discharge regime. As shown in Figure 4, where part of the long-term discharge and corresponding biomass time series are reported, the temporal fluctuations of flume discharge are reflected in the biomass temporal pattern. The numerical probability distribution function of biofilm biomass at equilibrium (i.e. for $t \to \infty$) correspondent to each light and discharge treatment was also assessed. As displayed in Figure 4, the biomass pdfs for the stochastic discharge regime are almost comparable for their shape and range interval, although shifted towards lower biomass values with decreasing light availability. No significant biomass differences emerged between the two discharge regimes. In particular, the differences between the equilibrium biomass value under the constant discharge regime and the average biomass value obtained from the stochastic discharge sequence were negligible among all light treatments (i.e. less than 0.1%), possibly because of the selected constant flow regime that was equal to the average value of the stochastic process.

DISCUSSION AND CONCLUSIONS

Bulk growth of benthic biofilms in experimental flumes was used to test a set of models, simulating growth dynamics. Forty different models have been defined for describing growth and loss dynamics. The MCMC algorithm has been applied to find the best set of parameter values for each model combination, and the AIC test has been performed in order to rank the models in terms of performances. Key processes controlling biofilm growth dynamics have been pointed out: Light and space limitation effects influenced the growth phase, while the hydraulic environment enhanced biomass losses because of detachment. Concerning the description of growth dynamics, we found that a linear light-dependent growth function could not properly describe photo-inhibition and photo-limitation processes measured during our experiment, whereas either

a saturating (Monod-type equation) or a hump-shaped relation (Steele's equation) seemed to perform comparably well. Analysing biomass loss dynamics, no clear differences among the performed loss models were found, probably because of biofilm suitability to experimental flow conditions and limited range of explored discharges. More specifically, given the limited experimental range of performed discharges, comprised between 0.1 and $0.51\,s^{-1}$, it is likely that biofilm was able to adapt and acclimate, by structural differentiation and viscoelastic properties, to the hydraulic conditions in the flumes, which did not impose extreme discharge events. The experiment was designed to avoid the lowest values of discharge, which are associated to very limited stages and would have induced an increased biofilm mortality. Moreover, the similar performance of the tested loss functions may stem from the fact that our experimental data did not yet show clearly the asymptote of the saturating behaviour associated with the balance of growth and loss. Therefore, alternative longer-lasting experimental designs should be exploited in the future in order to properly analyse hydraulic-induced biofilm loss dynamics and possibly characterise relevant influences of flow regime on stream ecosystems. However (see Supplementary Figure S1), the limits to growth were observed, and thus, the confidence in the predictive power of all models is granted.

The numerical analysis of the long term discharge sequence revealed interesting growth patterns. Whereas at low discharge values biofilm growth is enhanced, or at least preserved, discharge peaks induce a biomass decrease. Biofilm temporal fluctuations are slightly damped with respect to discharge variability, showing that biofilm does not immediately respond to discharge variations. Indeed, we found that the interplay between discharge and biofilm growth takes place at different temporal scales, of the order of hours for discharge and days for biofilm growth processes. We acknowledge that these considerations are specific to the case at hand, as biofilms in natural stream ecosystems are frequently disturbed by grazers and high discharge events.

The experimental and theoretical framework put together here, where the role of natural streamflow and light variability on stream biofilm dynamics has been analysed, is designed to handle all possible generalisations. In particular, from the bulk of our results, it is suggested that the definition of environmental flows suited to preserve riverine ecosystem services should not be based simply on the compliance of minimum flow requirements, as commonly held, but should rather take properly into account the natural variability of discharges within the range actually experienced by the river.

ACKNOWLEDGEMENTS

The authors thank the insightful comments of two anonymous reviewers. S. C., E. B., L. M. and A. R. gratefully acknowledge the support provided by ERC advanced grant programme through the project RINEC-227612 and by the SFN/FNS projects 200021_124930 and 200020_140661. T. J. B. acknowledges the financial support from FWF (STARTY420-B17). M. G. acknowledges the support of SNF/FNS project IZK0Z2_139537/1 for international cooperation. G. B. acknowledges the financial support from the Research Programme of the University of Padova CPDA105501/10. The authors declare to have no conflicts of interest.

REFERENCES

Akaike H. 1974. New look at statistical-model identification. *IEEE Transactions on Automatic Control* **19**(6): 716–723.

Allan J, Castillo M. 2007. *Stream Ecology: Structure and Function of Running Waters*. Springer: Dordrecht, The Netherlands.

Battin T, Kaplan L, Findlay S, Hopkinson C, Marti E, Packman A, Newbold J, Sabater F. 2008. Biophysical controls on organic carbon fluxes in fluvial networks. *Nature Geoscience* **1**(2): 95–100.

Biggs B. 1996. Hydraulic habitat of plants in streams. *Regulated Rivers: Research & Management* **12**(2-3): 131–144.

Biggs B, Close M. 1989. Periphyton biomass dynamics in gravel bed rivers – the relative effects of flows and nutrients. *Freshwater Biology* **22**(2): 209–231.

Biggs B, Duncan M, Jowett I, Quinn J, Hickey C, Daviescolley R, Close M. 1990. Ecological characterization, classification, and modeling of New-Zealand rivers – an introduction and synthesis. *New Zealand Journal of Marine and Freshwater Research* **24**(3): 277–304.

Biggs B, Goring D, Nikora V. 1998. Subsidy and stress responses of stream periphyton to gradients in water velocity as a function of community growth form. *Journal of Phycology* **34**(4): 598–607.

Biggs B, Nikora V, Snelder T. 2005. Linking scales of flow variability to lotic ecosystem structure and function. *River Research and Applications* **21**(2-3): 283–298.

Botter G, Basso S, Porporato A, Rodriguez-Iturbe I, Rinaldo A. 2010. Natural streamflow regime alterations: damming of the Piave river basin (Italy). *Water Resources Research* **46**: W06522.

Botter G, Peratoner F, Porporato A, Rodriguez-Iturbe I, Rinaldo A. 2007a. Signatures of large-scale soil moisture dynamics on streamflow statistics across US climate regimes. *Water Resources Research* **43**(11): W11413.

Botter G, Porporato A, Daly E, Rodriguez-Iturbe I, Rinaldo A. 2007b. Probabilistic characterization of base flows in river basins: roles of soil, vegetation, and geomorphology. *Water Resources Research* **43**(6): W06404.

Botter G, Porporato A, Rodriguez-Iturbe I, Rinaldo A. 2007c. Basin-scale soil moisture dynamics and the probabilistic characterization of carrier hydrologic flows: slow, leaching-prone components of the hydrologic response. *Water Resources Research* **43**(2): W02417.

Botter G, Zanardo S, Porporato A, Rodriguez-Iturbe I, Rinaldo A. 2008. Ecohydrological model of flow duration curves and annual minima. *Water Resources Research* **44**(8): W08418.

Burnham K, Anderson D. 2002. *Model Selection and Multimodel Inference: a Practical Information-Theoretic Approach*. Springer-Verlag: New York, N.Y., USA.

Carr J, D'Odorico P, McGlathery K, Wiberg P. 2012. Stability and resilience of seagrass meadows to seasonal and interannual dynamics and environmental stress. *Journal of Geophysical Research-Biogeosciences* **117**: G01007.

Ceola S, Botter G, Bertuzzo E, Porporato A, Rodriguez-Iturbe I, Rinaldo A. 2010. Comparative study of ecohydrological streamflow probability distributions. *Water Resources Research* **46**: W09502.

Corani G, Gatto M. 2007. Structural risk minimization: a robust method for density-dependence detection and model selection. *Ecography* **30**: 400–416.

DeNicola D, McIntire C. 1991. Effects of hydraulic refuge and irradiance on grazer–periphyton interactions in laboratory streams. *Journal of the North American Benthological Society* **10**(3): 251–262.

Ensign S, Doyle M, Piehler M. 2012. Tidal geomorphology affects phytoplankton at the transition from forested streams to tidal rivers. *Freshwater Biology* **57**(10): 2141–2155.

Fovet O, Belaud G, Litrico X, Charpentier S, Bertrand C, Dauta A, Hugodot C. 2010. Modelling periphyton in irrigation canals. *Ecological Modelling* **221**(8): 1153–1161.

Gilks W, Richardson S, Spiegelharter D. 1995. *Markov Chain Monte Carlo in Practice*. Chapman and Hall: New York.

Hastings W. 1970. Monte Carlo sampling methods using Markov chains and their applications. *Biometrika* **57**: 97–109.

Hill W, Ryon M, Schilling E. 1995. Light limitation in a stream ecosystem – responses by primary producers and consumers. *Ecology* **76**(4): 1297–1309.

Hondzo M, Wang H. 2002. Effects of turbulence on growth and metabolism of periphyton in a laboratory flume. *Water Resources Research* **38**(12): 1277.

Horner R, Welch E, Seeley M, Jacoby J. 1990. Responses of periphyton to changes in current velocity, suspended sediment and phosphorus concentration. *Freshwater Biology* **24**(2): 215–232.

Jackson R, Carpenter S, Dahm C, McKnight D, Naiman R, Postel S, Running S. 2001. Water in a changing world. *Ecological Applications* **11**(4): 1027–1045.

Jowett I, Duncan M. 1990. Flow variability in New-Zealand rivers and its relationship to in-stream habitat and biota. *New Zealand Journal of Marine and Freshwater Research* **24**(3): 305–317.

Julian J, Doyle M, Stanley E. 2008. Empirical modeling of light availability in rivers. *Journal of Geophysical Research-Biogeosciences* **113**(G3): G03022.

Kupferberg S, Palen W, Lind A, Bobzien S, Catenazzi A, Drennan J, Power M. 2012. Effects of flow regimes altered by dams on survival, population declines, and range-wide losses of California river-breeding frogs. *Conservation Biology* **26**(3): 513–524.

Lamberti G, Resh V. 1985. Comparability of introduced tiles and natural substrates for sampling lotic bacteria, algae and macroinvertebrates. *Freshwater Biology* **15**(1): 21–30.

Marks J, Power M, Parker M. 2000. Flood disturbance, algal productivity, and interannual variation in food chain length. *Oikos* **90**(1): 20–27.

McIntire C. 1973. Periphyton dynamics in laboratory streams – simulation model and its implications. *Ecological Monographs* **43**(3): 399–420.

Metropolis N, Rosenbluth A, Rosenbluth M, Teller A, Teller E. 1953. Equations of state calculations by fast computing machines. *Journal of Chemical Physics* **21**: 1087–1092.

Momo F. 1995. A new model for periphyton growth in running waters. *Hydrobiologia* **299**(3): 215–218.

Poff N, Allan J, Bain M, Karr J, Prestegaard K, Richter B, Sparks R, Stromberg J. 1997. The natural flow regime. *Bioscience* **47**(11): 769–784.

Poff N, Olden J, Merritt D, Pepin D. 2007. Homogenization of regional river dynamics by dams and global biodiversity implications. *Proceedings of the National Academy of Sciences of the United States of America* **104**(14): 5732–5737.

Power M, Parker G, Dietrich W, Sun A. 1995a. How does floodplain width affect river ecology – a preliminary exploration using simulations. *Geomorphology* **13**(1-4): 301–317.

Power M, Sun A, Parker G, Dietrich W, Wootton J. 1995b. Hydraulic food-chain models. *Bioscience* **45**(3): 159–167.

Richter B, Baumgartner J, Powell J, Braun D. 1996. A method for assessing hydrologic alteration within ecosystems. *Conservation Biology* **10**(4): 1163–1174.

Richter B, Baumgartner J, Wigington R, Braun D. 1997. How much water does a river need? *Freshwater Biology* **37**(1): 231–249.

Rinaldo A, Banavar J, Maritan A. 2006. Trees, networks, and hydrology. *Water Resources Research* **42**(6): W06D07.

Rinaldo A, Rodriguez-Iturbe I. 1996. Geomorphological theory of the hydrological response. *Hydrological Processes* **10**(6): 803–829.

Sabo J, Finlay J, Kennedy T, Post D. 2010. The role of discharge variation in scaling of drainage area and food chain length in rivers. *Science* **330**(6006): 965–967.

Saravia L, Momo F, Lissin L. 1998. Modelling periphyton dynamics in running water. *Ecological Modelling* **114**(1): 35–47.

Steele J. 1962. Environmental control of photosynthesis in the sea. *Limnology and Oceanography* **7**(2): 137–150.

Steele J, Baird I. 1962. Further relations between primary production, chlorophyll, and particulate carbon. *Limnology and Oceanography* **7**(1): 42–47.

Stevenson R. 1983. Effects of current and conditions simulating autogenically changing microhabitats on benthic diatom immigration. *Ecology* **64**(6): 1514–1524.

Stevenson R, Bothwell M, Lowe R. 1996. *Algal Ecology: Freshwater Benthic Ecosystems*. Academic Press: San Diego, CA.

Storn R, Price K. 1997. Differential Evolution – a simple and efficient heuristic for global optimization over continuous spaces. *Journal of Global Optimization* **11**: 341–359.

ter Braak C, Vrugt J. 2008. Differential evolution Markov chain with snooker updater and fewer chains. *Statistics and Computing* **18**: 435–446.

Tuji A. 2000. The effect of irradiance on the growth of different forms of freshwater diatoms: implications for succession in attached diatom communities. *Journal of Phycology* **36**(4): 659–661.

Uehlinger U, Buhrer H, Reichert P. 1996. Periphyton dynamics in a floodprone prealpine river: evaluation of significant processes by modelling. *Freshwater Biology* **36**(2): 249–263.

Vannote R, Minshall G, Cummins K, Sedell J, Cushing C. 1980. River continuum concept. *Canadian Journal of Fisheries and Aquatic Sciences* **37**(1): 130–137.

Vrugt J, ter Braak C, Diks C, Robinson B, Hyman J, Higdon D. 2009. Accelerating Markov chain Monte Carlo simulation by differential evolution with self-adaptive randomized subspace sampling. *International Journal of Nonlinear Sciences and Numerical Simulation* **10**: 271–288.